

• 工程结构减震与隔震 •

DOI:10.12454/j.jsuese.202301072



本刊网刊

新型旋转碰撞阻尼器控制性能研究与应用初探

沈均杰,王菁菁*

(广州大学 土木工程学院,广东 广州 510006)

摘要:提出一种新型控制装置——旋转碰撞阻尼器(RID),该装置基于两类质量阻尼器发展而成,由若干旋转体组成,各旋转体在同一平面内绕一固定轴旋转,相邻旋转体发生碰撞从而耗散能量,避免结构产生过大的加速度。首先,介绍RID的工作原理,建立非碰撞状态下主体结构和RID各旋转体的运动方程,建立碰撞状态下考虑相邻旋转体碰撞时动量守恒和恢复系数的碰撞模型;其次,通过动力试验比较RID的试验响应和数值响应,验证RID理论模型的准确性;再次,将结构简化为单向振动结构,采用脉冲型荷载对RID装置参数进行数值优化;最后,通过数值模拟方法对RID在柔性结构和刚性结构中的减振性能与应用展开研究。结果表明:在柔性结构的减震控制中,RID在地震响应与优化响应幅值相近时减震效果显著,但作为被动控制装置,RID发挥减振效果需要一定时间,且减振性能对地震时域特点和地震大小较敏感。因此,RID的减振性能仍有提升空间。在刚性结构的共振响应控制中,RID减振性能不受结构动力特性改变的影响,且所需的空行程不随激励增大而增长。此外,较大激励作用下,RID控制的主体结构呈现出强调制响应,该非线性动力响应有助于脉冲型荷载作用下的能量传递。

关键词:振动控制;旋转型质量阻尼器;碰撞型质量阻尼器;参数优化

中图分类号:O328;O322

文献标志码:A

文章编号:2096-3246(2025)04-0080-09

调谐质量阻尼器(TMD)是一种常见的被动控制技术^[1-4],在国内外实际工程中得到了广泛应用^[5-6]。TMD由附加质量块、线性弹簧和阻尼单元组成,一般安装在减振结构响应最大处,如高层建筑顶部^[7-8]。TMD能够与主体结构发生共振,共振引起TMD剧烈振动,从而消耗系统能量,减小主体结构响应。但TMD的减振性能依赖于调谐程度^[9-10],一旦TMD自振频率偏离主体结构自振频率,其减振性能会下降甚至加大主体结构响应^[11-13]。为此,Vakakis等^[14]提出非线性能量阱(NES),该装置用非线性刚度单元代替TMD中的线性刚度单元。由于NES产生的恢复力与其位移3次方成比例,附加质量块没有固定的共振频率,因此NES能与广泛的频率发生共振并且吸收能量^[15-17]。但由于非线性过强,NES的减振性能对输入荷载大小较为敏感,且上述3次方NES的运动轨迹为直线,只能控制单一方向的振动^[18-20]。而旋转NES由偏心附加质量组成,以转角为运动变量,在主体结构振动激励下,偏

心质量在水平面内发生转动,转动产生的作用力可以减小主体结构在任意水平方向的振动^[21-23]。但旋转NES的减振性能与其运动形式有关,只有发生大幅转动(而非小幅摆动)才能保证良好的效果^[24-26]。在增加耗能效率方面,碰撞NES通过附加质量与结构上的碰撞面发生碰撞而大量耗能,当激励大小超过引发碰撞的阈值时,碰撞NES在不同的能量等级均展现出优越的减振性能^[27-30]。然而,碰撞NES在碰撞瞬间会直接对主体结构施加较大的冲击力,从而使主体结构加速度剧增,造成局部构件损伤和人体舒适度降低等问题。为了综合旋转NES能够减小任意水平方向振动和碰撞NES耗能显著的优势,同时避免装置与结构直接碰撞的负面影响,Wang等^[31]提出了一种新型旋转碰撞阻尼器。本文对RID的工作原理、运动方程、碰撞模型进行分析和推导,提出参数数值优化方法,通过动力试验验证了RID模型的准确性,并基于数值模拟,对RID减振应用展开初步探索和研究。分析RID对地

收稿日期:2023-12-27 修回日期:2024-02-22 网络出版日期:2024-05-15

基金项目:国家自然科学基金面上项目(52078151);广东省基础与应用基础研究基金委员会面上项目(2023A1515012930;2024A1515010869)

作者简介:沈均杰(2000—),男,硕士生。研究方向:结构振动控制。E-mail:shenj755@163.com

*通信作者:王菁菁,副教授,E-mail:wangjj@gzhu.edu.cn

震作用下柔性结构和简谐荷载激励下刚性结构的控制效果和特点。结果表明:RID在地震响应与优化响应振幅相似时,其控制效果较为显著;RID的共振响应控制性能相比TMD更稳定,且所需的空间行程更小。

1 旋转碰撞阻尼器

1.1 工作原理

RID基于旋转NES及碰撞NES开发而成。该装置由多个旋转体(即偏心质量)组成,旋转体在同一个平面内绕固定轴旋转(图1)。当相邻旋转体间距减小为0时即发生碰撞。图1中, m_s 、 c_s 、 k_s 分别为主体结构质量、阻尼系数、刚度系数, x_s 为主体结构相对于地面的位移, m_R 为旋转体质量, θ_i 为第*i*个旋转体的角位移。

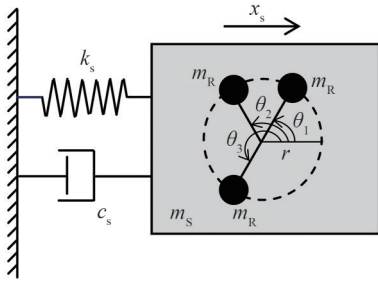


图1 单自由度结构附加RID理论模型

Fig. 1 Schematic of RID on a single-degree-of-freedom structure

RID的工作原理分为非碰撞和碰撞两个方面。首先,在非碰撞状态下,RID与旋转NES的运动相似,适用于结构在任意方向的振动,且其空间需求只与旋转体半径有关,因此不会随着激励的增加而增加。其次,在碰撞状态下,RID与碰撞NES相似,在碰撞瞬间能够大量消耗能量。但与碰撞NES不同,RID的碰撞发生在装置内部相邻旋转体之间,其冲击力不是直接作用于结构,因此能够避免引起过大的结构加速度。

1.2 运动方程

将RID安装于图1的单自由度主体结构,假设各旋转体参数完全相同,系统中阻尼作用均简化为线性黏滞阻尼。没有发生碰撞时主体结构和RID中各旋转体运动方程分别为^[31]:

$$(m_s + nm_R)\ddot{x}_s + c_s\dot{x}_s + k_s x_s = m_R \sum_{i=1}^n \frac{d}{dt}(\dot{\theta}_i \sin \theta_i) \quad (1)$$

$$m_R r^2 \ddot{\theta}_i + c_R \dot{\theta}_i = m_R r \ddot{x}_s \sin \theta_i, i = 1, 2, \dots, n \quad (2)$$

式(1)、(2)中, \ddot{x}_s 、 \dot{x}_s 分别为主体结构相对于地面的加速度、速度, c_R 、 r 分别为旋转体阻尼系数、旋转体半径, $\ddot{\theta}_i$ 、 $\dot{\theta}_i$ 分别为第*i*个旋转体的角加速度、角速度, n 为旋转体的数量。

将各旋转体的作用力之和视为施加在结构质量上的外力。

1.3 碰撞模型

当RID中相邻的旋转体发生碰撞时,其运动状态遵循动量守恒定律,并考虑恢复系数,可表示为:

$$\dot{\theta}_i^- + \dot{\theta}_j^- = \dot{\theta}_i^+ + \dot{\theta}_j^+ \quad (3)$$

$$r_c = -\frac{\dot{\theta}_i^+ - \dot{\theta}_j^+}{\dot{\theta}_i^- - \dot{\theta}_j^-} \quad (4)$$

式(3)、(4)中: $\dot{\theta}_i^-$ 和 $\dot{\theta}_j^-$ 分别为第*i*个和第*j*个旋转体碰撞前的运动状态; $\dot{\theta}_i^+$ 和 $\dot{\theta}_j^+$ 分别为第*i*个和第*j*个旋转体碰撞后的运动状态; r_c 为碰撞恢复系数,与碰撞表面材料及旋转体的质量和速度相关, $0 < r_c < 1$ 。

2 装置试验及模型验证

2.1 装置设计

小尺度RID试验模型如图2所示。RID旋转体由轴套(两个)、螺杆和转动轴承组装而成,三者固定连接形成刚体,绕中心杆转动。其中:两个轴套上下紧密连接,组成旋转质量;螺杆一端与旋转质量固定连接,另一端通过转动轴承套于中心杆上。轴套和转动轴承采用铝合金制成,螺杆采用钢材制成。RID试验模型包含3个相同的旋转体(R1~R3),通过数值模拟试算,确定RID对主体结构有较好控制效果的旋转体质量和半径(即从中心杆到轴套中心的距离)的范围。旋转体的质量约取试验中主体结构质量的1%,为0.621 kg(即每个旋转体质量为0.207 kg),半径约取试验中主体结构高度的1%,均为0.052 m。3个转动体的螺杆与各自转动轴承的连接位置相同,与各自旋转质量的连接位置不同,在高度上存在差异,以达到旋转质量位于同一高度,各旋转轴承位于中心杆不同高度的目的,使相邻转动体能够在转动过程中发生碰撞。

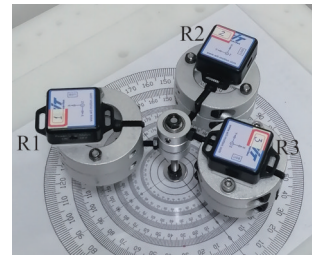


图2 RID试验模型

Fig. 2 Experimental model of RID

2.2 试验结果

基于RID的运动方程和碰撞模型,建立RID装置的MATLAB数值模型。通过对比RID在初始条件激励下的试验响应和数值模拟响应,检查数值模型的有效性,从而验证理论模型的正确性。试验中,通过无线陀螺仪测量各旋转体的转动角度和转动角速度。首先,在中心杆上每次安装单个旋转体,使单个旋转体发生

自由转动,识别其阻尼系数。得到R1~R3旋转体阻尼系数分别为 13×10^{-4} 、 2×10^{-4} 和 $3 \times 10^{-4} \text{ N} \cdot \text{m} \cdot \text{s}$ 。其次,在中心杆上每次安装两个旋转体,推动其中一个,使两者发生碰撞,识别其碰撞恢复系数,得到3个旋转体两两之间碰撞恢复系数均为0.15。最后,在中心杆上安装3个旋转体,推动其中一个,使其与另外两个发生碰撞,采集试验响应。同时,将3个旋转体的初始角度和初始角速度代入数值模型,得到相同试验条件下RID数值模型的转动角度和转动角速度响应。图3对比了3个旋转体的试验和数值模拟响应,由于RID在动力作用下的碰撞是随机的,基于统计意义的数值模型与试验结果存在合理范围内的误差,但两类响应变化趋势相同,数值结果能够从转动角度和转动角速度两方面较精确地反映真实结果,验证了数值模型的有效性和理论模型的正确性。RID数值模型将用于后续数值模拟研究。

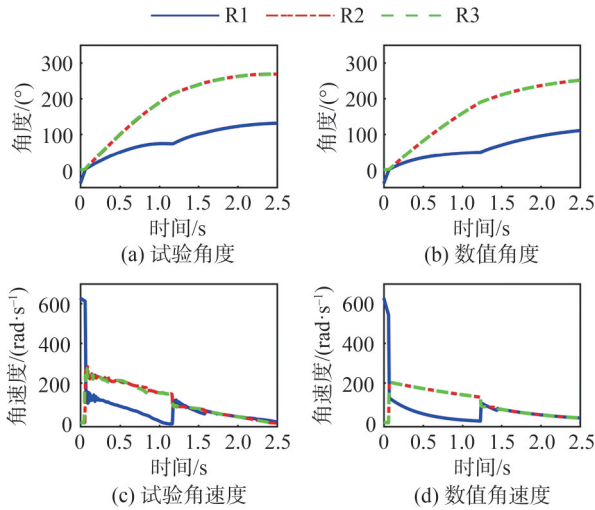


图3 试验和数值模拟响应对比

Fig. 3 Experiment and numerical simulation response comparison

3 控制参数优化方法

作为对RID振动控制可能性的初步探索,本文未涉及针对特定结构和荷载的设计方法,仅考虑单向振动或双向动力特性相近的主体结构,简化为单向振动结构,采用数值方法在简单激励作用下对RID控制参数进行优化。数值优化思路流程图如图4所示。第1步,给定RID质量 m_R 、旋转体的碰撞角度和碰撞恢复系数 r_c 。RID质量通常占主体结构质量的1%~5%。碰撞角度指碰撞发生时两旋转体质心的间隔角度,与旋转体尺寸有关。在碰撞质量相等的情况下,可认为碰撞恢复系数仅与碰撞面材料有关。第2步,根据碰撞角度确定各旋转体的可能初始角度。在静止条件下,RID中各旋转体处于随遇平衡状态,即旋转体可能停留在任意

位置。为考虑旋转体初始角度的随机性,需列出各旋转体初始角度的所有可能组合,作为后续数值模拟的初始条件。第3步,RID的待优化控制参数为旋转体半径 r 和阻尼系数 c_R ,设定两个参数的考察范围。第4步,在第3步所设定的范围内选取一对旋转体半径和阻尼系数,对主体结构施加初始位移激励,使结构按基本自振频率发生自由振动,通过数值模拟得到第2步中所有可能初始角度条件下的结构响应。第5步,计算各初始角度条件下结构响应的均方根,并计算所有初始角度条件下该均方根的平均值,作为所选取旋转体半径和阻尼系数对应的减振指标。第6步,遍历所有旋转体半径和阻尼系数,重复第4、5步,优化目标使减振指标达到最小值,此最小值对应的旋转体半径和阻尼系数,即为该RID的最优控制参数。值得注意的是,由于实际工程涉及不同的材料特性、荷载特性及主体结构特性,因此装置的最优参数在不同的工程中也需相应地调整。RID具有控制效果稳定且所需行程小的特点,这正是许多工程中所需要的。在未来研究中,将探索最优参数对不同工程条件的鲁棒性,分析其共性和差异,为实际不同工程提供更准确、更可行和更方便的参数优化方法。

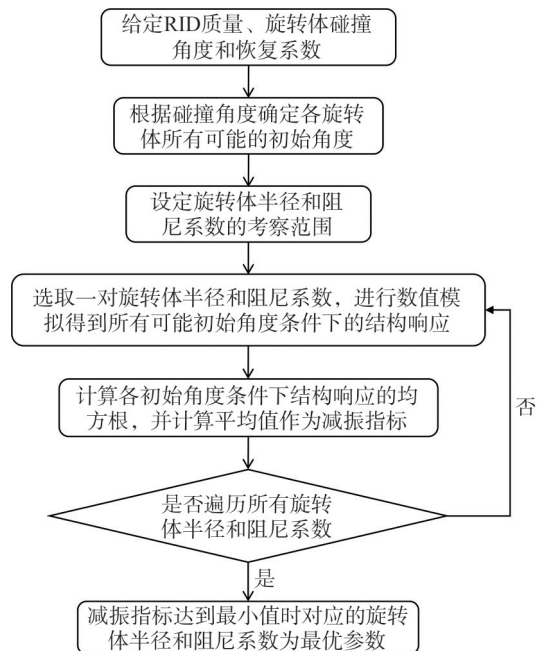


图4 RID优化思路流程图

Fig. 4 Flow chart of RID optimization

4 RID减振性能

以具有3个旋转体的RID为例,考察RID的减振控制性能。为探索RID潜在应用场景,选取两个主体结构:一个为周期大于1s的柔性结构,如风力机结构,考察RID的减震性能;另一个为周期小于1s的刚性结

构,如机械设备,考察简谐共振激励下RID的减振性能。

4.1 柔性结构减震控制

4.1.1 主体结构

柔性主体结构采用美国可再生能源部(NREL) 5 MW 水平风力机,该机型塔筒高为 87.6 m,结构总重 708 566 kg,1 阶振型为塔筒前后振动,自振周期为 3.12 s,其他参数见文献[32]。由于有限元模型难以模拟RID的非线性运动和碰撞行为,本文以文献[32-33]中 OPENFAST 模型为基准,建立 SAP2000 有限元模型,并基于 SAP2000 模型简化得到 10 个质点的层串模型,用于 MATLAB 数值模拟(图 5)。不同风力机模型响应对比如图 6 所示,对比了 OPENFAST 和 SAP2000 模型、SAP2000 和 MATLAB 模型的响应,各模型响应吻合良好。结构模态阻尼比取 0.5%,对应地震发生时风力机停机状态。该风力机双向动力特性相近,本文柔性结构减震控制研究中将风力机简化为单向振动 10 自由度主体结构进行分析。

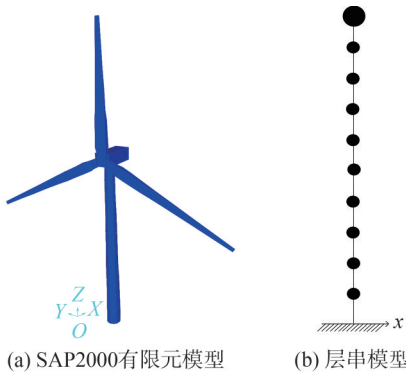


图 5 5 MW 水平风力机模型示意图

Fig. 5 Simulation models of 5 MW wind turbine

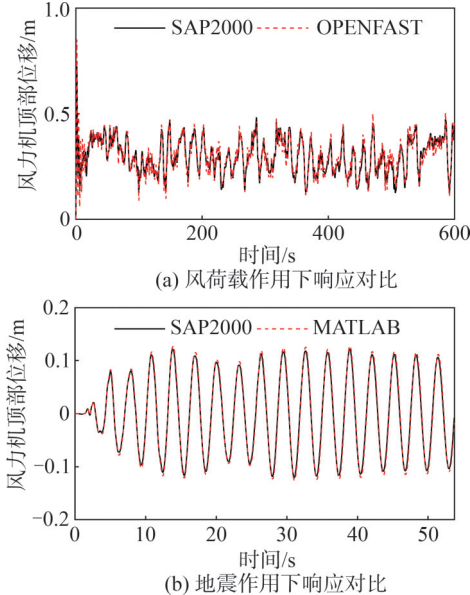


图 6 不同风力机模型响应对比

Fig. 6 Response comparisons between different wind turbine models

4.1.2 RID 参数优化

采用第 3 节的数值优化方法,选定 RID 质量为主体结构质量的 5%,为 35 428.32 kg(一个旋转体为 11 809.44 kg),并将其安装于风力机顶部,碰撞角度为 35°,碰撞恢复系数为 0.1,共取 77 组初始角度组合。对主体结构顶部施加 0.8 m 的初始位移,使结构发生大幅振动。对旋转体半径和阻尼系数进行优化,优化目标为主体结构顶层位移在初始 60 s 内的均方根达到最小值。得到 RID 最优半径为 1 m,阻尼系数为 2 362 N·m·s。图 7 为优化荷载作用下,未安装(无控)和安装(受控)优化后 RID 的风力机顶部的位移响应。

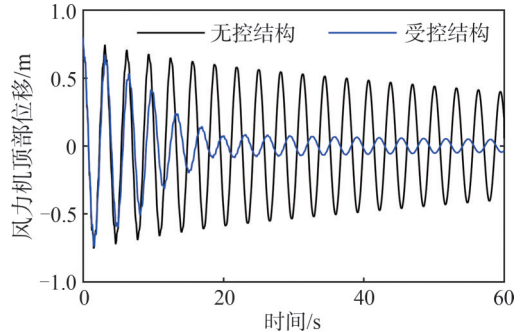


图 7 优化条件下风力机顶部位移响应

Fig. 7 Top displacements of wind turbine in the optimization

4.1.3 地震响应分析

为分析地震作用下 RID 的控制性能,选取 3 条代表性地震记录(表 1),对地震地面峰值加速度(PGA)进行缩放,以使结构响应与优化荷载作用下响应大小相符,对应强震激励。另外,风力机结构在地震作用结束时仍保持较强的振动,因此在地震记录原有持时上增加 60 s,作为计算时长。

表 1 地震信息

Tab. 1 Earthquake information

编号	地震	年份	测站	PGA	持时/s
1	Imperial Valley	1940	El Centro Array#9-270	0.5g	53.46
2	Northridge	1994	Newhall-Fire Sta-90	1.0g	40.00
3	Kobe Japan	1995	KJMA	2.0g	150.00

图 8 以 RID 初始角度 0°、45° 和 90° 为例,显示了 3 条地震作用下 RID 各旋转体的旋转角度和无控及受控风力机顶层位移时程,RID 旋转角度中的竖向虚线表示碰撞。2 号地震作用下碰撞过于密集,为清晰展示,图 8(b)仅绘制了 RID 在部分时段的旋转角度和碰撞。由图 8 可以发现,由于 RID 是一种被动控制装置,在地震作用初期控制效果不明显,随着 RID 开始旋转及碰撞,受控结构顶层位移在 40 s 时均减小至无控结构的 60% 以下。另外,RID 控制效果受到地震时域特点的影响,当地震峰值出现在地震初期时 RID 控制效果较好,而地震幅值反复波动时控制效果较差。

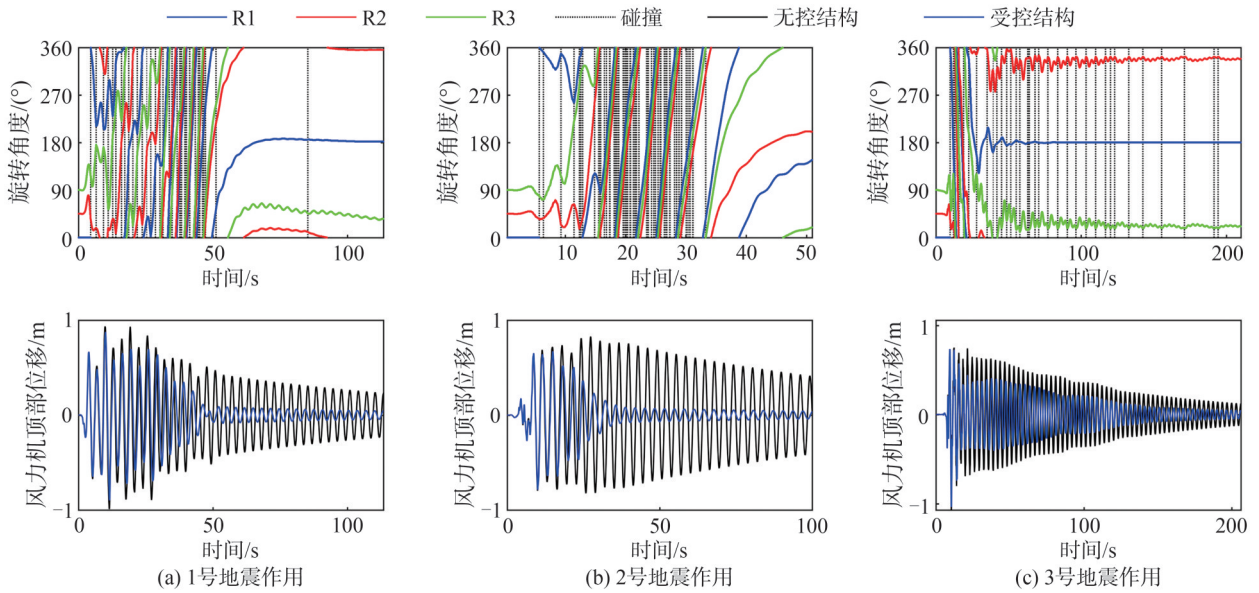


图8 地震作用下RID的旋转、碰撞及结构顶层位移对比

Fig. 8 Comparison of rotation, collision, and top displacements of RID under seismic ground motions

图9显示了当3条地震作用PGA减小一半时，RID的旋转角度和无控及受控风力机顶层位移时程，以模拟激励小于优化荷载等级的情况。可以发现，当激励减小时，RID没有充分旋转和碰撞，控制效果显著退化，在1号地震作用下甚至增大了结构顶层位移

响应。由此可知，RID对能量输入有较强的依赖性，不适合激励能量范围广泛且无法预测的情况。对于能量、频谱和时域特点均具有较大随机性的地震作用，现有的RID控制方法仍不完备，有待未来研究的优化和改进。

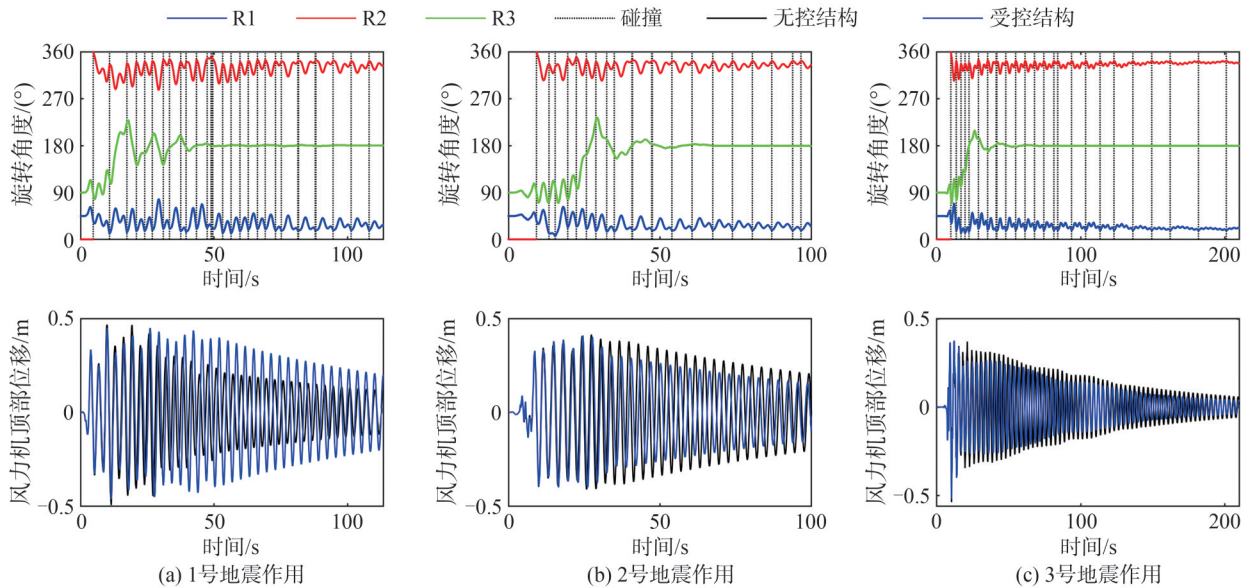


图9 减弱地震作用下RID的旋转、碰撞及结构顶层位移对比

Fig. 9 Comparison of rotation, collision, and top displacements of RID under reduced seismic ground motions

4.2 刚性结构减振控制

4.2.1 主体结构

刚性主体结构以文献[31]中的两自由度试验结构为原型，结构的总重为7.10 kg，1阶自振周期为0.52 s，模态的阻尼比为0.38%，符合机械设备阻尼小、共振响应大的特点。同时，考虑到机械设备因负荷、夹持松紧和出力不同，导致结构动力特性发生改变，因此，除原

结构外，还将考察自振周期减小至原结构周期的67%、50%和40%这三种结构。4种结构按周期从大到小编号为结构1~4。需要指出的是，真实机械设备的自振周期和振动幅值一般远小于文献[31]中的试验结构，因此，本文仅从类比的角度考察当主体结构特性发生显著改变时，旋转碰撞阻尼器RID对共振响应的控制效果。

4.2.2 RID参数优化

RID 安装于结构中振动最显著的末端质量,选定 RID 质量为主体结构质量的 5%,碰撞角度为 75°,碰撞恢复系数为 0.1,共取 82 组初始角度组合。优化采用的主体结构为自振周期不发生改变的结构 1,对结构末端质量施加 40 mm 初始位移,对旋转体半径和阻尼系数进行优化,优化目标为主体结构末端质量位移在初始 20 个周期内(约 10 s)的均方根达到最小值。得到 RID 最优半径为 0.05 m,阻尼系数为 $3.54 \times 10^{-4} \text{ N} \cdot \text{m} \cdot \text{s}$ 。图 10 为优化荷载作用下,未安装(无控)和安装(受控)了优化后 RID 的结构末端质量的位移响应。

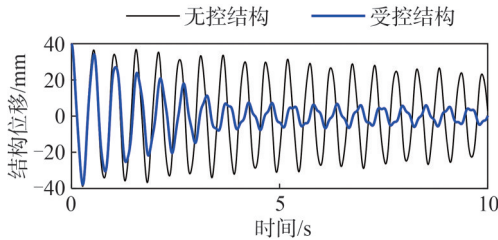


图 10 优化条件下无控结构和受控结构末端位移响应
Fig. 10 Uncontrolled and controlled structural displacements in the optimization

4.2.3 共振响应分析

考察简谐基底位移激励作用下,RID 对共振响应的控制效果。为说明 RID 减振控制特点,共振响应分析中还考虑了质量比同为 5% 的 TMD。TMD 采用和 RID 相同的主体结构、安装位置、荷载和响应指标进行数值优化,得到 TMD 最优刚度系数为 45 N/m,阻尼系数为 1.06 N·s/m。

图 11 以 RID 初始角度 45°、101°和 337°为例,显示了基底位移幅值为 0.3 mm 时,无控和受控结构末端质量的共振位移时程。此时,各结构基底位移的振动周期与结构 1 阶自振周期相同,结构响应出现最大值。对比 4 种结构的响应可知:TMD 在结构 1 上展现出极佳的减振性能,这是由于 TMD 基于结构 1 优化得到,与结构 1 相调谐。但随着结构自振周期降低,TMD 与结构失谐,其控制性能逐步退化。而与之相对的,RID 的减振效率基本不受结构动力特性变化的影响,虽然 RID 的控制效果不及调谐时的 TMD,但在结构动力特性可能发生大幅改变的情况下,RID 较 TMD 展现出更加稳定的减振能力。

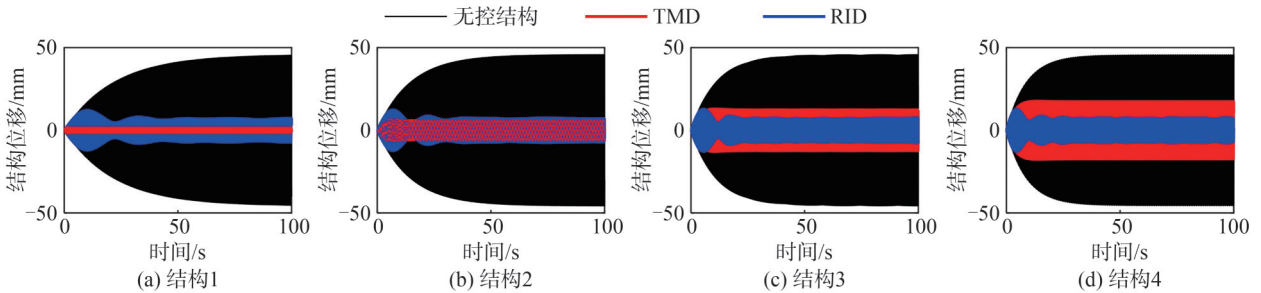


图 11 简谐地面位移(0.3 mm)激励下结构末端质量共振响应对比

Fig. 11 Comparison of resonant structural responses under harmonic ground displacement (0.3 mm)

图 12 显示了基底位移幅值为 1.0 mm 时,无控和受控结构末端质量的共振位移时程。与图 11 观察到的结果相同,调谐的 TMD 减振效果优于 RID,而 RID 能够在不同结构中维持相似的减振效率,具有较强的稳定性。同时,RID 控制下的主体结构展现出强调制响应,即结构的稳态响应幅值交替增减,是典型的非线性

性动力响应,有助于脉冲型荷载作用下能量从结构到装置的单向传递,应在未来 RID 研究中予以关注。最后,值得指出的是,RID 的运动始终局限于其半径范围内($r=0.05 \text{ m}$),其空间需求不随荷载增加而增加,而 TMD 的行程在 1.0 mm 基底位移激励下已到达 0.14 m,且随荷载增加继续增长。

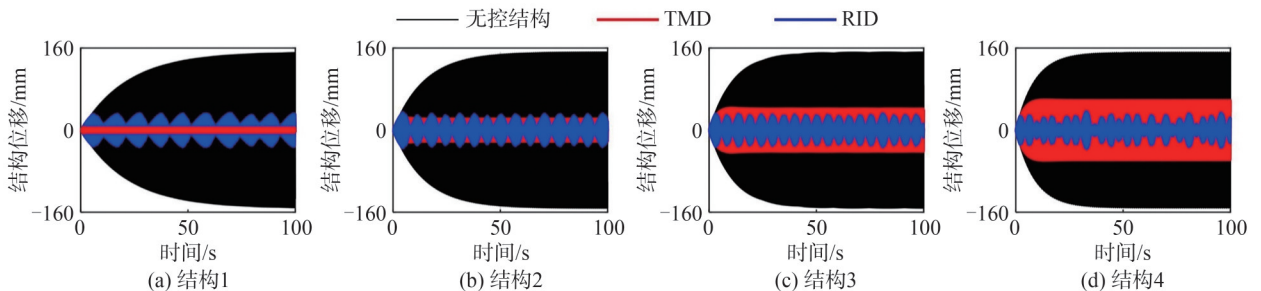


图 12 简谐地面位移(1.0 mm)激励下结构末端质量共振响应对比

Fig. 12 Comparison of resonant structural responses under harmonic ground displacement (1.0 mm)

5 结 论

本文提出了一种新型旋转碰撞阻尼器。RID 由 3 个绕同一固定轴的旋转体组成,相邻旋转体在荷载激励下发生旋转和碰撞从而耗散能量,且不会在结构中引起过大的加速度。首先,介绍了 RID 的工作原理和理论模型;其次,对 RID 理论模型进行了试验验证,提出了 RID 控制参数数值优化方法;最后,使用经过验证的数值模型,对 RID 在柔性结构和刚性结构的减振性能和应用进行了分析。结果表明:

1)在柔性结构减震控制中,当地震响应与优化响应幅值相近时,RID 减震效果明显;但同时,RID 作为被动控制装置,需要一定的反应时间,且减震性能受地震时域特点的影响。

2)当地震作用大幅减小时,RID 的旋转运动和碰撞减少,导致控制效果显著退化,即 RID 对能量输入具有较强的依赖性。考虑到地震作用的随机性,RID 的减震控制性能仍有待改进。

3)在刚性结构共振响应控制中,在结构动力特性不变时,RID 的减振性能不及 TMD,但随着结构动力特性的改变,TMD 的控制效果逐渐减弱,而 RID 的减振效果几乎不受结构动力特性变化的影响,展现出更稳定的减振性能。

4)RID 的空间需求不随荷载增加而增加,相比之下,TMD 的行程随荷载增加而增长;且在较大激励作用下,RID 控制的主体结构呈现出强调制响应,该非线性动力响应有助于脉冲型荷载作用下的能量传递,应在未来 RID 研究中予以关注。

参考文献:

[1] Soong T T, Spencer B F. Supplemental energy dissipation: State-of-the-art and state-of-the-practice[J]. *Engineering Structures*, 2002, 24(3): 243–259.

[2] Li Chunxiang, Liu Yanxia, Wang Zhaomin. A review on mass dampers[J]. *Advances in Mechanics*, 2003, 33(2): 194–206. [李春祥, 刘艳霞, 王肇民. 质量阻尼器的发展[J]. *力学进展*, 2003, 33(2): 194–206.]

[3] Wang Jungang, Ma Rujian, Zhao Dong, et al. Development and application of TMD structural vibration control[J]. *Journal of Jinan University (Science and Technology)*, 2006, 20(2): 172–175. [王均刚, 马汝建, 赵东, 等. TMD 振动控制结构的发展及应用[J]. *济南大学学报(自然科学版)*, 2006, 20(2): 172–175.]

[4] Gao Yang, Zhai Endi, Li Shuanghu, et al. Integrated design and real-world application of a tuned mass damper(TMD) with displacement constraints for large offshore monopile wind turbines[J]. *Ocean Engineering*, 2024, 292: 116568.

[5] Jin C, Chung W C, Kwon D S, et al. Optimization of tuned mass damper for seismic control of submerged floating tunnel[J]. *Engineering Structures*, 2021, 241: 112460.

[6] Lin Y Y, Cheng C M, Lee C H. A tuned mass damper for suppressing the coupled flexural and torsional buffeting response of long-span bridges[J]. *Engineering Structures*, 2000, 22(9): 1195–1204.

[7] Xu Kun, Bi Kaiming, Han Qiang, et al. Using tuned mass damper inerter to mitigate vortex-induced vibration of long-span bridges: Analytical study[J]. *Engineering Structures*, 2019, 182: 101–111.

[8] Zhang Hang, Wen Binrong, Tian Xinliang, et al. Experimental study on mitigating vibration of floating offshore wind turbine using tuned mass damper[J]. *Ocean Engineering*, 2023, 288: 115974.

[9] Liu Xingyan. Research on damping performance and influence factors of tmd structure[J]. *Industrial Construction*, 2016, 46(7): 124–128. [刘兴彦. 调谐质量阻尼器结构减震性能及影响因素研究[J]. *工业建筑*, 2016, 46(7): 124–128.]

[10] Tong Changhong, Zhang Xiaodong. Parameter optimization of toned mass dampers and its application to bridge vibration[J]. *Journal of Vibration, Measurement & Diagnosis*, 2007, 27(2): 146–149. [同长虹, 张小栋. 调谐质量阻尼器参数优化及其应用[J]. *振动、测试与诊断*, 2007, 27(2): 146–149.]

[11] Wang Liangkun, Shi Weixing, Wang Hongtao, et al. An adaptive-passive tuned mass damper system[J]. *Journal of Vibration, Measurement & Diagnosis (Natural Science Edition)*, 2019, 39(4): 781–788. [王梁坤, 施卫星, 王洪涛, 等. 自适应 TMD 减振性能试验[J]. *振动、测试与诊断*, 2019, 39(4): 781–788.]

[12] Rana R, Soong T T. Parametric study and simplified design of tuned mass dampers[J]. *Engineering Structures*, 1998, 20(3): 193–204.

[13] Chen Yiming, Jin Xin, Liu Hao, et al. Large scale wind turbine TMD optimization based on Blade–Nacelle–Tower–Foundation Coupled Model[J]. *Ocean Engineering*, 2021, 239: 109764.

[14] Vakakis A F. Inducing passive nonlinear energy sinks in vibrating systems[J]. *Journal of Vibration and Acoustics*, 2001, 123(3): 324–332.

[15] Zang Jian, Zhang Yewei, Ding Hu, et al. The evaluation of a nonlinear energy sink absorber based on the transmissibility[J]. *Mechanical Systems and Signal Processing*, 2019, 125: 99–122.

[16] Liu Zhongpo, Lu Xilin, Lu Zheng, et al. Experimental investigation on vibration control effect of track nonlinear energy sink[J]. *Journal of Building Structures*, 2016, 37(11): 1–9. [刘中坡, 吕西林, 鲁正, 等. 轨道型非线性能量阱振动控制

- 的振动台试验研究[J]. 建筑结构学报,2016,37(11):1-9.]
- [17] Shi Chenglong, Zhang Jigang, Cheng Yun. Research progress of nonlinear energy sink vibration reduction[J]. Earthquake Engineering and Engineering Dynamics, 2021, 41(2): 162-174. [时成龙, 张纪刚, 程贇. 非线性能量阱减振的研究进展[J]. 地震工程与工程振动, 2021, 41(2): 162-174.]
- [18] Wang Jingjing, Liu Zhibin, Hao Wenming. Innovative nonlinear structural control methods for seismic response reduction[J]. Journal of Vibration and Shock, 2019, 38(12): 32-38. [王菁菁, 刘志彬, 浩文明. 非线性-线性联合结构控制方法减震性能研究[J]. 振动与冲击, 2019, 38(12): 32-38.]
- [19] Ndemanou B P, Ndoukouo A N, Metsebo J, et al. Nonlinear energy sink response of a cylindrical storage tank under earthquake loads[J]. Soil Dynamics and Earthquake Engineering, 2024, 179: 108536.
- [20] Wang Hongli, Ding Hu. Vibration reduction of floating raft system based on nonlinear energy sinks[J]. Ocean Engineering, 2023, 288: 116211.
- [21] AL-Shudeifat M A, Wierschem N E, Bergman L A, et al. Numerical and experimental investigations of a rotating nonlinear energy sink[J]. Meccanica, 2017, 52(4): 763-779.
- [22] Blanchard A, Bergman L A, Vakakis A F. Vortex-induced vibration of a linearly sprung cylinder with an internal rotational nonlinear energy sink in turbulent flow[J]. Nonlinear Dynamics, 2020, 99(1): 593-609.
- [23] Ding Ke, Pearlstein A J. Free response of a rotational nonlinear energy sink: Complete dissipation of initial energy for small initial rectilinear displacements[J]. Journal of Applied Mechanics, 2021, 88(1): 011005.
- [24] Gendelman O V, Sigalov G, Manevitch L I, et al. Dynamics of an eccentric rotational nonlinear energy sink[J]. Journal of Applied Mechanics, 2012, 79(1): 011012.
- [25] Sigalov G, Gendelman O V, AL-Shudeifat M A, et al. Resonance captures and targeted energy transfers in an inertially-coupled rotational nonlinear energy sink[J]. Nonlinear Dynamics, 2012, 69(4): 1693-1704.
- [26] Selwanis M M, Franzini G R, Béguin C, et al. Multi-ball rotative nonlinear energy sink for galloping mitigation[J]. Journal of Sound and Vibration, 2022, 526: 116744.
- [27] AL-Shudeifat M A, Wierschem N, Quinn D D, et al. Numerical and experimental investigation of a highly effective single-sided vibro-impact non-linear energy sink for shock mitigation[J]. International Journal of Non-Linear Mechanics, 2013, 52: 96-109.
- [28] Wang Jingjing, Wierschem N, Spencer B F, et al. Numerical and experimental study of the performance of a single-sided vibro-impact track nonlinear energy sink[J]. Earthquake Engineering & Structural Dynamics, 2016, 45(4): 635-652.
- [29] Wang Jingjing, Zhang Chao, Li Haobo, et al. A vertical-vibro-impact-enhanced track bistable nonlinear energy sink for robust and comprehensive control of structures[J]. Structural Control and Health Monitoring, 2022, 29(5): 114137.
- [30] Feudo S L, Job S, Cavallo M, et al. Finite contact duration modeling of a Vibro-Impact Nonlinear Energy Sink to protect a civil engineering frame structure against seismic events[J]. Engineering Structures, 2022, 259: 114137.
- [31] Wang Jingjing, Zheng Yuqiang, Ma Yuhong. Experimental study on rotational impact dampers[J]. Mechanical Systems and Signal Processing, 2023, 204: 110805.
- [32] Jonkman J, Butterfield S, Musial W, et al. Definition of a 5-MW reference wind turbine for offshore system development: Technical report NREL/TP-500-38060[R]. Golden: National Renewable Energy Laboratory, 2009.
- [33] Alotta G, Biondo C, Giaralis A, et al. Seismic protection of land-based wind turbine towers using the tuned inerter damper[J]. Structures, 2023, 51: 640-656.

Control Performance and Preliminary Application Investigation of Novel Rotational Impact Dampers

SHEN Junjie, WANG Jingjing*

(School of Civil Engineering, Guangzhou University, Guangzhou 510006, China)

Abstract:

Objective A new type of control device, the Rotational Impact Damper (RID), is proposed. This device is developed based on two types of mass dampers and consists of multiple rotating bodies that rotate about a fixed axis within the same plane. Adjacent rotating bodies rotate and collide when excited, dissipating energy without inducing excessive acceleration in the structure.

Methods Firstly, the working principle of RID was introduced. The working principle of RID was divided into two aspects, namely, non-collision and collision states. For the non-collision state, the equations of motion (EOMs), including the EOM for the main structure and the EOMs for each rotating body in RID, were established. For the collision state, a collision model was established. In particular, when adjacent rotating bodies collided in RID, their motion followed the law of conservation of momentum and accounted for the coefficient of restitution. Secondly, dynamic tests were conducted to compare the experimental and numerical responses of three rotating bodies. As the collision of RID under dynamic loading was random, the numerical responses were not the same as the experimental responses. However, remarkable similarities were observed in their response tendencies and statistics. Therefore, it was considered that the numerical results accurately reflected the physical reality, predicting

the rotation angle and rotational angular velocity with relatively good consistency. Following the verification of the effectiveness of the numerical model and the correctness of the theoretical model, the numerical model of the RID was used for subsequent numerical simulation research. Thirdly, for main structures with similar dynamic properties in the two horizontal directions, a simplification was conducted to model the structure as a unidirectional structure. Numerical optimization was conducted to determine the control parameters of the RID under simple excitation. The numerical optimization method was divided into six steps. Step 1: RID mass, rotational collision angle, and recovery coefficient were set. Step 2: All possible initial angles for each rotating body were determined based on the collision angle. Step 3: The inspection range for the radius and damping coefficient of the rotating body was set. Step 4: A pair of rotating body radius and damping coefficients were selected for the numerical simulation, and the structural response under all possible initial angle conditions was obtained. Step 5: The root mean square of the structural response under various initial angle conditions was calculated, and the average value was taken as the vibration reduction index. Step 6: all radii and damping coefficients of the rotating body were traversed, repeating the fourth and fifth steps, with the optimization goal of achieving the minimum vibration reduction index. The radius and damping coefficient of the rotating body corresponding to this minimum value were the optimal control parameters for this RID. Finally, to explore the potential application scenarios of RID, two main structures were selected and analyzed through numerical simulation. The first structure was a flexible structure with a period greater than 1 second, such as a wind turbine structure. The finite element model of the wind turbine structure was established in SAP2000 finite element software, and the finite element model was simplified as a lumped-mass model with 10 degrees of freedom for MATLAB numerical simulation. Three representative earthquake records were selected to analyze the control performance of RID under seismic excitations, and the peak ground accelerations were scaled to match the structural response under the load used in the optimization, corresponding to strong seismic excitations. In addition, the wind turbine structure maintained strong vibration even after the earthquake, so an additional 60 seconds were added to the original earthquake records. The other study investigated the RID vibration reduction performance when applied to a rigid structure (such as mechanical equipment) with a period of less than 1 second under harmonic resonance excitation. Considering the changes in the structural dynamic characteristics of mechanical equipment due to differences in load, clamping tightness, and output, this study also examined three additional structures with natural vibration periods reduced to 67%, 50%, and 40% of the original structure period, in addition to the original structure. A tuned mass damper (TMD) with a mass ratio of 5% was also considered in the resonance response analysis to study the control effect of RID on resonance response under harmonic base displacement excitation and to explain the characteristics of RID vibration reduction control. TMD was numerically optimized using the same primary structure, installation position, load, and response indicators as RID.

Results and Discussions The analysis results indicate that in the seismic control of flexible structures, when the seismic response closely aligns with the optimized response amplitude, the seismic reduction effect of the RID is substantial. However, as a passive control device, the RID requires a specific response time, and its seismic performance is influenced by the time-domain characteristics of earthquakes. Furthermore, a considerable reduction in seismic effects leads to decreased rotational motion and fewer collisions of the RID, which results in a significant degradation in control effectiveness and highlights the RID's strong dependence on energy input. Given the stochastic nature of seismic excitations, the seismic control performance of the RID still presents opportunities for improvement. In the context of resonance response control for rigid structures, when the structural dynamic characteristics remain unchanged, the vibration reduction performance of the RID is not as strong as that of the TMD. However, as the structural dynamic characteristics vary, the effectiveness of the TMD gradually diminishes, whereas the vibration reduction capability of the RID remains largely unaffected by such changes, demonstrating a more stable vibration reduction performance. Additionally, the spatial requirements of the RID do not increase with growing loads, unlike those of the TMD, for which the stroke increases proportionally with the load increment. Under significant excitation, the primary structure controlled by the RID exhibits strongly modulated responses that facilitate targeted energy transfer under impulsive loads, emphasizing the necessity for further investigation in future RID research efforts.

Conclusions In summary, the RID shows significant seismic reduction effects when seismic responses approximate optimized amplitudes, especially in flexible structures. The RID's performance is influenced by earthquake time-domain characteristics and depends heavily on energy input due to reduced rotational motion and collisions under diminished seismic effects. While it is less effective than TMDs under unchanged structural dynamics in rigid structures, the RID maintains stable vibration reduction as structural characteristics vary and does not require increased spatial capacity with load increments. The strongly modulated responses under high excitations enhance targeted energy transfer, illustrating the RID's potential and the need for continued research. These findings underline the RID's theoretical and practical value in seismic control applications.

Key words: vibration control; rotating mass damper; impact mass damper; parameter optimization

(编辑 周璇)

引用格式: Shen Junjie, Wang Jingjing. Control performance and preliminary application investigation of novel rotational impact dampers[J]. *Advanced Engineering Sciences*, 2025, 57(4): 80–88. [沈均杰, 王菁菁. 新型旋转碰撞阻尼器控制性能研究与应用初探[J]. *工程科学与技术*, 2025, 57(4): 80–88.]